Elastic properties of hollow colloidal particles

C. I. Zoldesi,[1] I. L. Ivanovska,[2] C. Quilliet,[3] G. J. L. Wuite,[2] and A. Imhof[1,*]

[1]*Soft Condensed Matter, Debye Institute for Nanomaterials Science, Department of Physics and Astronomy, Utrecht University, Princetonplein 5, 3584 CC Utrecht, The Netherlands*

[2]*Faculty of Exact Sciences, Department of Physics and Astronomy, Vrije Universiteit, De Boelelaan 1081, 1081 HV Amsterdam, The Netherlands*

[3]*Laboratoire de Spectrométrie Physique, CNRS UMR 5588 and Université Joseph Fourier, 140 avenue de la Physique, 38402 Saint-Martin d'Hères Cedex, France*

(Received 30 July 2008; published 5 November 2008)

The elastic properties of micrometer-sized hollow colloidal particles obtained by emulsion templating are probed by nanoindentation measurements in which point forces are applied to solvent-filled particles supported on a flat substrate. We show that the shells respond linearly up to forces of 7–21 nN, where the indentation becomes of the order of the shell thickness (20–40 nm). In the linear region, the particle deformation is reversible. The measured Young's modulus (~200 MPa) is comparable to values for stiff rubbers or soft polymers. At larger applied force, we observe a crossover into a nonlinear regime, where the shells assume a buckled shape. Here, the force increases approximately as the square root of the indentation, in agreement with the theory of elasticity of thin shells. We also observe permanent deformation of the shells after probing them repetitively beyond the linear regime. Finally, the measured elastic properties of the shells nicely explain their spontaneous buckling in solution and due to drying.

DOI: 10.1103/PhysRevE.78.051401 PACS number(s): 82.70.Dd, 62.25.De, 68.37.Ps

I. INTRODUCTION

The importance of microcapsule systems for life-science applications in medicine, cosmetics, or the food industry has continuously increased. In general, microcapsules are used for controlled encapsulation and release of various agents. In view of the many diverse applications, there are also very different materials to be encapsulated and the requirements for these capsules vary drastically.

The physicochemical properties of polyelectrolyte multilayer capsules have been intensively investigated [1–7]; likewise biological capsules, such as virus capsids and cells, have been the subject of many studies as well [8–12]. Additionally, microcapsules have received significant attention from a theoretical point of view [13–18]. For many applications, the most important properties of a capsule are its wall permeability, adhesion, and mechanical behavior. In this work, we will focus on their mechanical properties, which are relevant for the elucidation of the deformation and adhesion behavior.

There have been several recent attempts to study the mechanical properties of various types of shells, and several techniques have been proposed. In general, we can distinguish between methods that use osmotic pressure effects to exert forces on the microcapsules [1,4,5], and methods that rely on the micromanipulation of individual capsules. Although the last category is technically more demanding, there is better control over the applied forces, a greater range of forces that can be tested, and the possibility to vary them *in situ*. Due to these advantages, atomic force microscopy has become a widely used technique to study the deformation of microcapsules [2,3,7,10,11,19].

The hollow colloidal particles we investigate consist of a cross-linked network of siloxane and silica. They are formed chemically using low molecular weight polydimethylsiloxane (oil) droplets as templates. The initial oil droplets can be removed easily by dissolution, as described in our previous work [20,21]. The resulting solvent-filled shells are highly monodisperse and their shell thickness can be varied over a considerable range. We have investigated the elastic properties of these thin-shelled particles using atomic force microscopy (AFM). This method allows us to determine how hollow shells respond to applied point forces, the types of deformation that appear, and permits us to extract their material properties. In this system, we have been able to observe the crossover from the regime of linear to that of nonlinear deformation. This takes place when the indentation becomes of the order of the shell thickness. In contrast to earlier work, in which a large spherical probe was used [1–3,7], a point force (i.e., AFM tip) allows for easier comparison of our result with existing analytical theory. Moreover, the buckled shell develops a symmetric, circular dimple instead of an asymmetric, wrinkled depression. Contrary to the sudden failure that is seen in viral shells at high applied forces [11,12], buckling of our shells is always smooth and continuous.

While the indentation experiments were all done on solvent-filled shells, buckling can also be induced by different methods, for instance when the templating oil droplet is removed by dissolution or evaporation. Using the measured elastic properties of the shells, we can attribute this buckling due to capillary forces that arise when the encapsulated liquid escapes the shell through pores of a few nanometers in size [22].

*Author to whom correspondence should be addressed. a.imhof@uu.nl

II. MATERIALS AND METHODS

A. Sample preparation

1. Samples for indentation experiments

The hollow shells used in the AFM experiments were prepared by an emulsion templating technique in which surfactant-stabilized emulsion droplets were incorporated in solid silica/siloxane shells, followed by removal of the core. This procedure is described in detail in Ref. [23]. In brief, an emulsion was prepared from 2% v/v dimethyldiethoxysilane (DMDES), 2% v/v concentrated ammonia (25%), and 0.002% w/w Triton X-100 surfactant. After 20 h, 0.02 M tetraethoxysilane (TEOS) was added. By taking samples after 3, 5, and 7 h and interrupting shell growth, we obtained three different sets of hollow silica/siloxane shells having the same core size but a different shell thickness. The particles were then washed several times with ethanol to remove the oil from the core, after which they were transferred to demineralized water. The size of the core and thickness of the shell, as well as size polydispersity, were measured with static light scattering (SLS) prior to the AFM experiments [20].

The samples used for AFM were prepared as follows: a droplet of 40 μL of the dispersion of shells in water was deposited on a glass slide (0.15 mm thickness and 22 mm diameter) mounted on the piezo holder. After deposition, the excess dispersion was gently removed with a Pasteur pipette, keeping the surface wet, and replaced by demineralized water. In order to attach the shells firmly to the surface, the glass slides were first coated with 3-aminopropyltriethoxysilane (APS) by keeping them for 1.5 h in a solution containing 170 mL ethanol, 4.5 mL of a 25% ammonia solution, and 23.5 mL APS, after which they were dried under nitrogen.

2. Samples for buckling experiments

To determine the buckling threshold in solution, we prepared larger polydimethylsiloxane (PDMS) droplets from 2% v/v DMDES and 2% v/v ammonia (in 25 mL total volume), with radii of 540, 650, and 690 nm, respectively. We added TEOS (0.018 M) 24 h after the emulsion preparation. We took samples at different times during shell growth (after 2.5, 7, 25, and 49 h, respectively) and we measured the shell thickness with static light scattering. The suspensions were then mixed with equal volumes of ethanol in order to induce buckling. All the observations discussed in Sec. III refer to samples for which we used 50% ethanol by volume.

B. Characterization

1. Atomic force microscopy

The indentation measurements were performed with an AFM (Nanotec, Madrid) operated in "jumping mode" in liquid [10,24]. In this mode, imaging is achieved by a succession of force-distance (FZ) curves to low maximal force ($<$0.2 nN), executed in several milliseconds in a raster scanning fashion. Lateral displacements occur only when the tip is not in contact with the sample, thereby minimizing shear forces. A complete description of the apparatus and the measurement procedure can be found in Ref. [24]. The maximal applied force is well defined because each individual approach is stopped at the cantilever deflection corresponding to the set force. FZ curves were recorded by measuring cantilever deflection (force) as a function of the vertical position of the Z-piezo to which the sample was mounted. The relation between the voltage output and the force was determined by making FZ measurements on the glass substrate surface next to the shells. FZ curves of the particles were recorded after positioning the AFM tip above the center of individual shells, which was located by stopping the cantilever in the middle of a topographical scan of a shell. The tip position was then fine-tuned by making a profile scan and by redirecting the tip to the middle of the shell cross section with an estimated deviation of less than about 5 nm. The FZ curves were recorded in slow mode ($\sim$1 s), in sequences of three successive curves. The experiments were performed in liquid (water) to investigate the shells in an undeformed state. The silicon cantilevers (OMCL-RC800PSA, Olympus, Tokyo) had nominal spring constants of 0.05, 0.1, 0.39, and 0.76 N/m, respectively. The spring constant of each batch is always calibrated before the experiments by means of the resonant frequency using the procedure described in Ref. [25]. The measured spring constants within a batch vary within 15–20 %. In addition, we determine tip radii for a batch of tips typically using viral particles with known size as calibration objects. The tip radii of the cantilevers used were $\sim$20 nm, in agreement with the value reported by the manufacturer.

2. Transmission optical microscopy

The buckled shells in solution were observed using a Leica confocal scanning microscope, type TCS-SP2 operated in transmission mode, using glass capillaries (0.1×2.0 mm) filled with the suspension.

3. Scanning electron microscopy (SEM)

SEM was used to study the deformation of the dried shells. The micrographs were obtained with a Philips XL 30 FEG scanning electron microscope and the samples were prepared by drying a drop of concentrated particle suspension on a glass slide.

III. RESULTS

A. Study of the buckling threshold

The microcapsules studied are prepared by synthesizing low molecular weight PDMS oil droplets, followed by a step that coats them with a thin shell of cross-linked siloxane and silica. The oil can then be removed so that spherical, solvent-filled shells remain. We distinguished in Ref. [20] three types of hollow particles depending on the shape they assume after drying them in air from an ethanol solution. We concluded that the main factor that influences particle behavior is the relative shell thickness d/R [21]. While shells with $d/R > 0.3$ remain spherical, those with a lower value consistently buckle to form hemispherical caps. Figure 1(a) is an illustra-

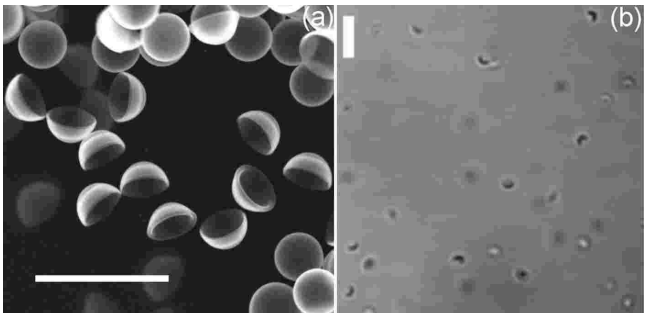

FIG. 1. (a) SEM image of hollow shells that buckled as a result of drying from ethanol; (b) transmission optical micrograph of a suspension of oil-filled colloidal silica/siloxane shells that buckled after ethanol had been added to the aqueous suspension. Scale bars are 5 μm.

tion of these particles. Shells with $d/R<0.05$ assume a more crumpled shape.

Interestingly, buckling could also be induced in solution by mixing suspensions of thin oil-filled shells in water with equal volumes of ethanol. Surprisingly, we observed that the shells all deformed permanently into a bowl-like shape, as shown in [Fig. 1(b)]. Since the particles in water never showed any such deformation, the buckling must occur due to the presence of ethanol. Being a good solvent for PDMS ethanol-dissolves the low molecular weight PDMS into the exterior medium, now consisting of an ethanol-water mixture. Using optical microscopy, we determined the percentage of buckled shells observed in suspensions of varying d/R. The results are presented in Fig. 2, each point corresponding to 40–80 objects. The relative thickness below which buckling occurs can thus be estimated at $(d/R)_{c,\text{solution}}=0.17$. Buckling of shells is expected to depend on the elastic properties of the material, most notably on Young's modulus. To measure this modulus, we performed AFM nanoindentation experiments.

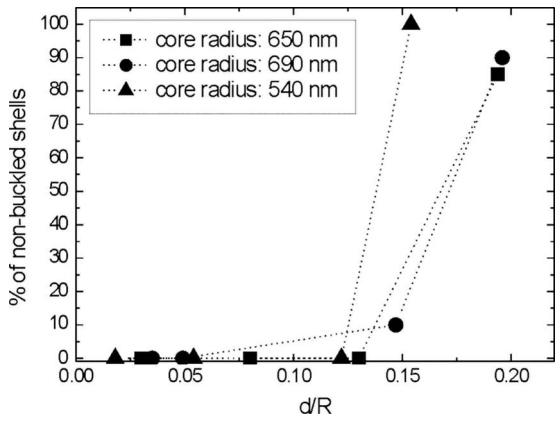

FIG. 2. Proportion of oil-filled shells in water retaining their spherical shape after an equal volume of ethanol had been added. The symbols represent the three different samples used in the experiment, with different core radius of the droplets used for encapsulation. Buckling suddenly occurs below a relative shell thickness $(d/R)_c \approx 0.17$.

TABLE I. Size and polydispersity of particles used in AFM experiments, as determined by SLS; R_c, core radius; d, shell thickness; δ, polydispersity in the total size; and R, average radius of the particle $(R=R_c+d/2)$.

Sample	R_c (nm)	d (nm)	δ (%)	d/R
Sa	265	17.5	9	0.06
Sb	265	27.5	9	0.09
Sc	265	37.5	9	0.12

B. Indentation experiments

AFM measurements were performed on different samples consisting of suspensions of hollow shells (filled with water) in water. An overview of the samples used in these experiments is given in Table I. They were all made with the same templating oil droplets but with different encapsulation thicknesses.

Imaging of the shells was first performed at low resolution and low maximal force (<0.2 nN) to determine their position. An example is shown in Fig. 3. The broad slopes seen around the particles are due to the convolution of the objects with the pyramidal shape of the tip. High-resolution scans of individual shells showed that most of them were intact (except for a small number of shells already deformed due to partial drying during sample preparation) and they were firmly attached to the glass surface. After individual objects had been imaged, indentation measurements were performed, following the procedure described in the experimental section.

In Fig. 4, three successive FZ curves on a single shell from sample Sa are shown. They were measured in the direction of approach ("forward"). For all measurements on the Sa sample, cantilevers with a spring constant of 0.05 N/m were used. Typically the Sa shells responded linearly to forces up to 6 ± 1 nN ($n=12$ shells measured). The indentation at this point is about 18 nm. We define the limit of linearity as the point where the derivative of the force-distance curve starts to deviate more than 10% from its value at the lowest forces.

The maximum force applied for this sample was ~11 nN. At this force, the shells were indented by 31 ± 4 nm ($n=12$), which represents about 6% of their total height. The shells still recover their initial shape after such deformation,

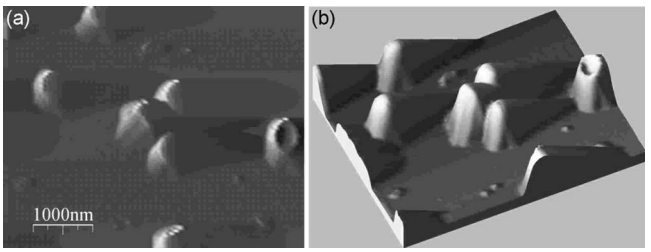

FIG. 3. Low-resolution AFM images of shells from sample Sc in water (scan area, 5 μm×5 μm, 128×128 pixels): (a) direct topographic image; (b) the same image in 3D representation. A collapsed particle can be seen on the right of the images.

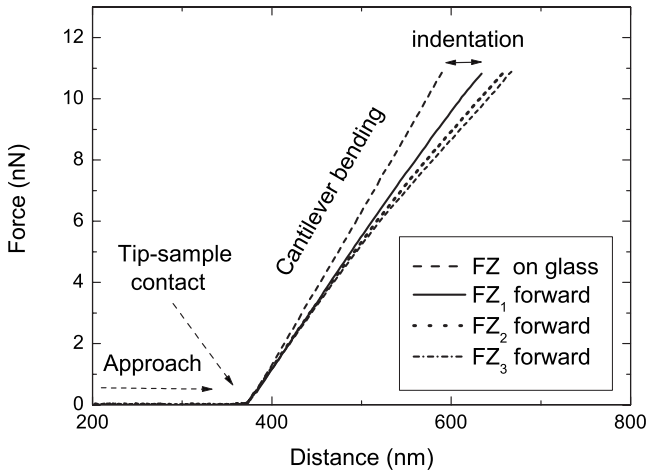

FIG. 4. Typical FZ indentation curves measured on a single shell from sample Sa. Distance represents the vertical z-piezo displacement. The leftmost dashed curve shows the cantilever on the glass surface. The glass curve was shifted along the z axis to match the tip-sample contact point of the shell allowing direct readout of the indentation of the shell resulting from the applied point force.

and images taken immediately after indentation showed no evidence of damage. However, we did detect a slight permanent softening of the objects after the first FZ curve as can be seen by the decrease in the slope of the FZ curves (see Fig. 4). This may be due to some plasticity of the shells in regions of high curvature. Therefore, to determine the elastic response of a shell, we always use the linear part of the first forward FZ curve (FZ_1).

The second sample (Sb, Table I) was measured using slightly stiffer cantilevers (0.1 N/m). Figure 5 shows an example of a particle from this sample. At forces beyond 10 ± 2 nN ($n=8$), or indentation of ~16 nm, deviations from linearity were observed with the slope of the FZ curves decreasing. The maximum force applied on these particles was ~25 nN and the deformation of these shells at this force was ~67 nm (about 12% of the total diameter). When indented so deeply, the shells were permanently deformed into an extensively buckled shape, as can be seen in Fig. 5.

The third sample (Sc, Table I) was measured using two different cantilever types, with spring constants of 0.39 and 0.76 N/m, which allowed us to apply maximum forces of ~50 and ~60 nN, respectively. The shells showed the same behavior in both cases: they responded linearly up to forces of 17 ± 3 nN ($n=15$), or indentation 14 nm, after which significant deviations from linearity were observed. A typical example of indentation of a shell from sample Sc is presented in Fig. 6. In this particular case, as a result of the applied force (using the 0.76 N/m cantilever), the maximum indentation achieved was ~110 nm (~18% of the total diameter). As can be seen from Fig. 6(c), this indentation resulted in a large permanent deformation, which explains the very different elastic response in the second and third FZ measurements.

Experiments performed on many shells from sample Sc, with both cantilevers, revealed a peculiar two-population distribution of particles. The objects in these populations appeared to respond slightly differently when the same forces

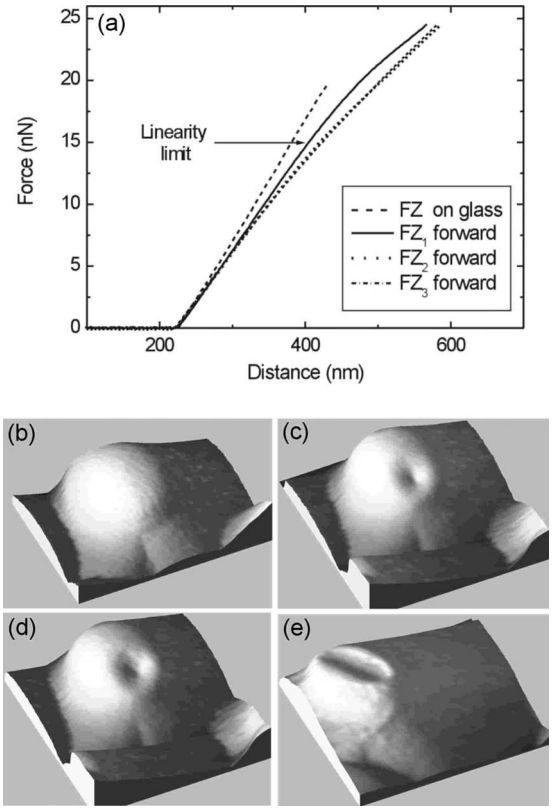

FIG. 5. (a) FZ indentation curves measured on a single shell from sample Sb; the leftmost dashed curve shows the FZ on the glass substrate. AFM images of the same particle are shown in (b) before indentation, (c) after the first FZ series, (d) after the second FZ series, and (e) after the third FZ series. The scan area is $1.3\ \mu m \times 1.3\ \mu m$.

were applied. This is illustrated in Fig. 7, in which we show two different objects from sample Sc, before and after we applied the same maximum force (~58 nN). The maximum indentation achieved was ~85 nm for object 1, and ~131 nm for object 2. Object 1 is clearly stiffer. Moreover, its linear regime extends to slightly larger forces compared to object 2. By measuring the height of the objects before indentation, we found a difference of ~10% between the height of the softer and stiffer objects. Therefore, the difference in stiffness probably stems from size bidispersity of the sample. In the analysis of the elastic response of the shells, we therefore treated sample Sc as two distinct populations, Sc1 and Sc2.

IV. DISCUSSION

A. Indentation experiments

The theory of elasticity of thin shells predicts a linear elastic response for the indentation of a homogeneous spherical shell up to an indentation magnitude (Δz) on the order of the shell thickness (d) [16,26], in which case the applied force (F) is

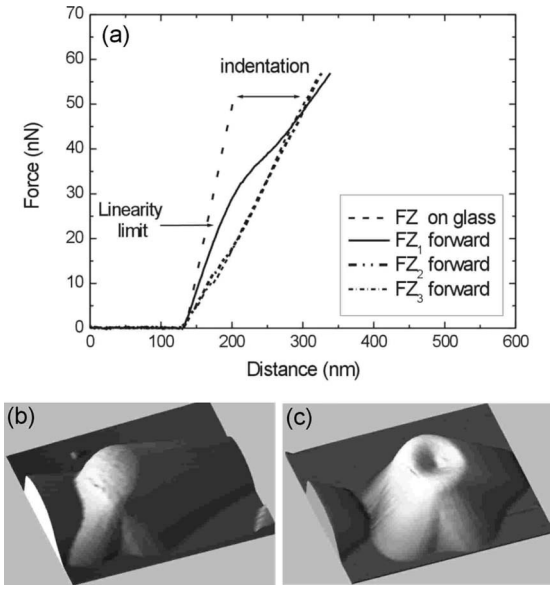

FIG. 6. (a) Forward FZ indentation curves performed on a shell from sample Sc (population 1). The AFM images show this shell (b) before and (c) after the FZ series. The scan area is 1.7 μm $\times$1.7 μm.

$$F \sim \frac{Ed^2}{R}\Delta z, \tag{1}$$

where E is Young's modulus and R is the average radius of the shell ($R_c+d/2$). The linear response we obtained for our shells, up to forces of several nN and at indentations $\Delta z < d$, indicates that they behave indeed as expected for such objects. Beyond this regime, nonlinear buckling is predicted because of the coupling between in-plane compression and out-of-plane bending. In this case, a circular cap is inverted leading to a buckled shape such as seen in Figs. 5(c) and 5(d). Most of the elastic energy is then stored as bending energy in the circular "bending strip," the radius of which grows with the indentation. Moreover, the magnitude of the applied point force is predicted to be [16,27]

$$F \sim \frac{Ed^{5/2}}{R}(\Delta z)^{1/2} \tag{2}$$

for deformations larger than the shell thickness. This agrees well with deviations from linearity observed in our measurements in the last part of the FZ curves.

Calculations have shown that deviations from thin shell theory begin to become noticeable only when d/R exceeds about $1/10$ [28]. We therefore expect this theory to hold for our samples.

In the case of deformation of a closed capsule, the question of their permeability or volume conservation must also be considered [29]. The volume of an impermeable shell filled with an incompressible fluid is constrained. This leads to an additional restoring force arising from the shell's stretching to keep its volume constrained while the spherical capsule is deformed. This contribution to the force is proportional to the third power of the indentation [29],

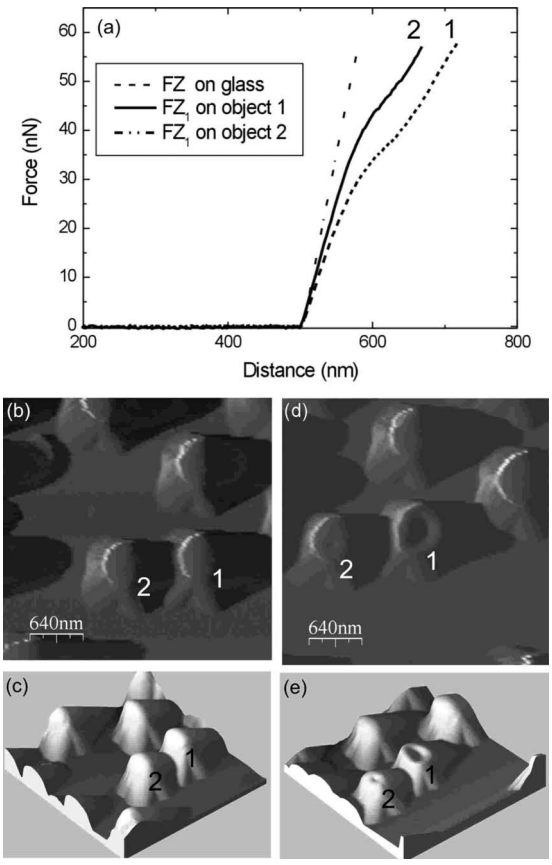

FIG. 7. (a) First forward FZ indentation curves performed on the objects 1 and 2 indicated in the AFM images. (b) Direct topographic image of shells from sample Sc in water before indentation. (c) The same image in 3D representation. (d) AFM image of the objects after the FZ series. (e) The same image in 3D representation.

$$F_{\text{volume}} \approx \frac{2\pi}{3}\frac{Ed}{R^2}E(\Delta z)^3. \tag{3}$$

Being of higher order, it should not affect the slope of the linear part of the FZ curves. Furthermore, this result predicts a steepening of the FZ curves with indentation, which was not observed in our experiments. On the contrary, we found a downward curvature of the FZ curves. This indicates that on the time scale of the indentation ($\sim$1 s), the shells must be fully permeable to the solvent.

Focusing on the regime of linear deformation now, we conclude that the elastic response can be described by that of a thin spherical shell undergoing small deformations, Eq. (1). The shell's spring constant can be related to Young's modulus, E, of the shell material,

$$F = k_{\text{shell}}\Delta z, \tag{4}$$

where the spring constant is known analytically [30,31],

$$k_{\text{shell}} = \frac{2E}{\sqrt{3(1-\sigma^2)}}\frac{d^2}{R}. \tag{5}$$

Here σ is the Poisson ratio. Spring constants of shells can be obtained from the slopes of the linear parts of the forward FZ curves. The shell's spring constant (k_{shell}) is then related to

TABLE II. Spring constants (k_{shell}, with standard deviation and number of particles measured) for samples Sa, Sb, and the two populations found in sample Sc, and the indentation up to which the shells still respond linearly to the applied force (Δz_{lin}).

Sample	k_{shell} (N/m)	Δz_{lin} (nm)
Sa	$0.33 \pm 0.04 (n=14)$	18
Sb	$0.57 \pm 0.08 (n=8)$	16
Sc1	$1.04 \pm 0.10 (n=6)$	13
Sc2	$1.50 \pm 0.10 (n=9)$	16

the effective spring constant k_{eff} (the slope of the FZ curve), and the cantilever spring constant k_c by [11]

$$k_{shell} = \frac{k_c k_{eff}}{k_c - k_{eff}}. \quad (6)$$

Mean values of the spring constant distributions for each sample measured are shown in Table II, and plotted in the histograms in Fig. 8. The values obtained for the spring constants clearly show an increase of the object stiffness with increasing shell thickness.

With Eq. (5), the measured k_{shell}, and the values of d and R obtained from Table I, we can estimate Young's modulus of the material making up the shells. Reasonably assuming that the shell consists of the same material in all three samples, we obtain a Young's modulus of 200 ± 40 MPa ($n=37$) overall. We assumed a Poisson ratio of 0.3, but the result depends very little on it. Considering that the density of the shell material is $\sim 1000\ \mathrm{kg/m^3}$ [32], our value for Young's modulus indicates that our shells are made of a material that is somewhere at the boundary between a stiff rubber and soft polymer [33]. This is not unexpected, considering that the shell is in fact a densely cross-linked organosilica network of silicate and dimethylsiloxane units [21]. Several factors are responsible for the considerable spread in the E values. First, the polydispersity in particle size (determined by light scattering) contributes to the spread in spring constants determined experimentally. Moreover, the size of the particle core was determined right before the encapsulation step and was used to determine the final size and polydispersity of the core-shell particles. Therefore, there is an uncertainty in the shell thickness that arises from the polydispersity of the core. This will show up in the E values, in which the shell thickness is present as d^2. Furthermore, the numerical prefactor in Eq. (5) depends slightly (about 10%) on d/R, and therefore also affects the E values [31]. Finally, we assume the same material for the shells in each case, but the pores can be distributed differently over the shell for different shell thickness and could lead to differences in Young's modulus.

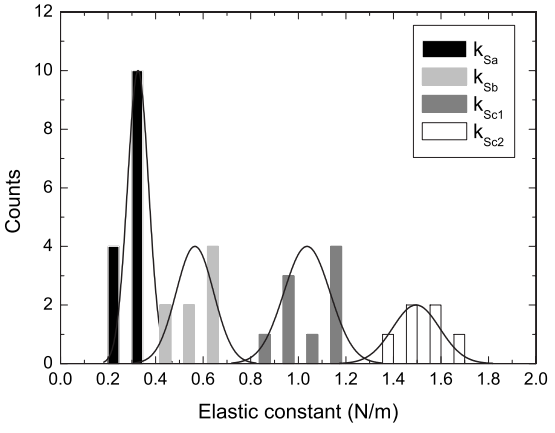

FIG. 8. Histograms of measured spring constants. The drawn lines are Gaussian fits.

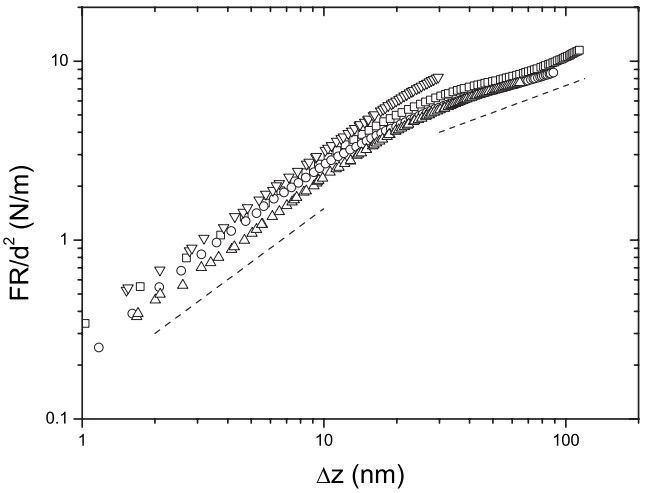

FIG. 9. Plot showing FR/d^2 vs indentation averaged over all measured particles in a sample. Down triangles, sample Sa; up triangles, sample Sb; circles and squares, sample Sc measured with 0.39 and 0.76 N/m cantilevers, respectively. The dashed lines have slopes of 1 and 1/2, respectively.

The nonlinear deformation of indented particles is best seen in a plot of F versus the indentation Δz. We calculated the indentation for each measurement by subtracting the z in the substrate measurement from the z in the sample measurement. We then averaged the resulting curves over all (about 10) measured particles in a sample. The resulting plot shown in Fig. 9 confirms the scaling of the force with d^2/R, albeit with a considerable spread in the data. At large indentations, the force increases approximately as $(\Delta z)^{1/2}$, as indeed Eq. (2) predicts. The crossover into this regime is smooth and continuous and takes place when the indentation approaches the shell thickness and the shell bends inward and forms the bending strip. This crossover has not been observed before, possibly due to the very high force resolution needed or the use of a large spherical bead as the indenter [1,7] constraining the size of the bending strip. We do not observe the expected systematic increase in Δz at crossover when the shell is made thicker. It is possible that this effect is obscured by our use of cantilever tips with radii of curvature (about 20 nm) that are themselves on the order of the shell thickness. The effect of tip size and shape on the crossover is hard to predict, but should no longer affect the scaling in Eq. (2) once the bending strip has grown larger, as is seen in Fig. 9.

B. Buckling threshold

The results of the indentation measurements shed light on the buckling of solvent-filled shells when they are dried or, in

the case of oil-filled shells, when the oil is extracted with a good solvent such as ethanol. Both times buckling takes place at a critical, though different, d/R.

This type of buckling can be explained by considering the same arguments used in the literature for buckling of spherical porous shells [17,34]. As the solvent enclosed by the shells begins to leave through pores in the shell, solvent-air (respectively oil-solvent) menisci in those pores grow hollow. This causes, for each pore, a global inward capillary force. At a larger scale, the effect is similar to an external effective pressure that reaches a maximal value of

$$p_{\mathrm{eff}} = \frac{4\gamma}{a}, \tag{7}$$

where γ is the interfacial tension and a is the typical diameter of the pores. For a spherical geometry, the occurrence of buckling of thin shells is predicted by elasticity theory to happen at a critical pressure of [26,27]

$$p_c = \frac{2E}{\sqrt{3(1-\sigma^2)}}\left(\frac{d}{R}\right)^2. \tag{8}$$

When effective pressure is realized through evaporation, this pressure cannot easily be varied, as it is fixed by the solvent and the porosity of the shell. However, we can tune the macroscopic geometry in order to determine the critical relative shell thickness $(d/R)_c$ below which buckling occurs. From Eqs. (7) and (8), the latter is expected to scale as

$$\left(\frac{d}{R}\right)_c = [2\sqrt{3(1-\sigma^2)}]^{1/2}\left(\frac{\gamma}{aE}\right)^{1/2}. \tag{9}$$

According to the diagram presented in Ref. [21], the relative thickness below which deformation occurs as a result of drying is $(d/R_t)_{c,\mathrm{air}} \approx 0.3$. Considering that for ethanol $\gamma = 22.4$ mN/m at 20 °C, we obtain from Eq. (9) the value $aE = 0.82$ J/m^2. With the measured Young's modulus of $E \approx 200$ MPa, the pore size can be approximated as $a \approx 4$ nm. This value is in good agreement with the permeability experiments presented in Ref. [21], from which we concluded that the diameter of the pores should be at least 1.1 nm to allow the dye molecule fluorescein isothiocyanate (FITC) to pass. On the other hand, pores had to be smaller than about 10 nm because they could not be resolved with transmission electron microscopy and AFM.

Alternatively, buckling could be induced in solution by mixing suspensions of thin oil-filled thin shells in water with equal volumes of ethanol, as shown in Fig. 1(b). In this case, we should expect that there is an interface between the remaining oil and the water/ethanol solvent in the pores. When the inner oil now dissolves into the external medium, one expects that a capillary pressure acts in the same way as during drying, and Eq. (9) is expected to remain valid with γ now representing the oil/solvent interfacial tension. The relative thickness below which buckling occurred was $(d/R)_{c,\mathrm{solution}} = 0.17$. With the value of aE determined above, we may then propose a value of $\gamma_{\mathrm{oil/water+ethanol}} = 7$ mN/m for the interfacial tension between the oil and a 50/50 water/ethanol mixture. This is consistent with the value $\gamma_{\mathrm{oil/water}} = 14$ mN/m determined for the same type of synthesized PDMS in water [35]. The addition of ethanol is expected to lower this value. Also, it is possible that the value of E is slightly modified because in this experiment the shell is in contact with a different solvent than in the drying experiment (ethanol plus water instead of just ethanol).

Finally, from these data we can also estimate the magnitude of the effective pressure acting on the particles when the inner oil dissolves into the external medium,

$$p_{\mathrm{eff}} = \frac{4\gamma_{\mathrm{oil/water+ethanol}}}{a} \approx 7 \text{ MPa}. \tag{10}$$

This corresponds to an osmotic pressure of a solution (assumed ideal) of 2.8 M concentration, which is quite significant and may even be increased by a judicious choice of the organic solvent.

V. CONCLUSIONS

We determined experimentally the elastic properties of micrometer-sized hollow silica/siloxane shells in a liquid and found that the deformation of these shells is well described by the elastic theory of thin shells. We investigated the response of the particles to an applied point force and found that the shells showed a perfect linear response and no permanent deformation when indented with depths approximately equal to the shell thickness. Above this value, the force increased with the square root of the indentation. At these forces, the shells suffered irreversible buckling leading to a dimpled shape. From the linear response, we determined the spring constant and found that the shells become stiffer for larger relative shell thicknesses, in agreement with findings from our previous work [20,21]. From the spring constant, we extracted Young's modulus of our shells $(200 \pm 40$ MPa). This value, together with the considerations concerning the density of the shell material, indicates that we are dealing with a material with elastic properties, somewhere between those of a soft polymer and a stiff rubber. Finally, the determined Young's modulus explains the buckling of the shells, both as a result of drying in air and in ethanol solution.

ACKNOWLEDGMENTS

This work was financially supported by the Nederlandse Organisatie voor Wetenschappelijk Onderzoek (NWO).

[1] O. I. Vinogradova, J. Phys.: Condens. Matter **16**, R1105 (2004).
[2] O. V. Lebedeva, B.-S. Kim, and O. I. Vinogradova, Langmuir **20**, 10685 (2004).
[3] V. V. Lulevich, D. Andrienko, and O. I. Vinogradova, J. Chem. Phys. **120**, 3822 (2004).
[4] V. V. Lulevich, I. L. Radtchenko, G. B. Skhorukov, and O. I. Vinogradova, J. Phys. Chem. B **107**, 2735 (2003).
[5] C. Gao, E. Donath, S. Moya, V. Dudnik, and H. Möhwald, Eur. Phys. J. E **5**, 21 (2001).
[6] S. Leporatti, C. Gao, A. Voigt, E. Donath, and H. Möhwald, Eur. Phys. J. E **5**, 13 (2001).
[7] F. Dubreuil, N. Elsner, and A. Fery, Eur. Phys. J. E **12**, 215 (2003).
[8] J. Guck, R. Ananthakrishnan, T. J. Moon, C. C. Cunningham, and J. Käs, Phys. Rev. Lett. **84**, 5451 (2000).
[9] R. Mukhopadhyay, G. Lim, and M. Wortis, Biophys. J. **82**, 1756 (2002).
[10] I. L. Ivanovska, P. de Pablo, B. Ibarra, G. Sgalari, F. MacKintosh, J. Carrasccosa, C. F. Schmidt, and G. J. L. Wuite, Proc. Natl. Acad. Sci. U.S.A. **101**, 7600 (2004).
[11] J. Michel, I. L. Ivanovska, M. Gibbons, W. Klug, C. Knobler, G. J. L. Wuite, and C. F. Schmidt, Proc. Natl. Acad. Sci. U.S.A. **103**, 6184 (2006).
[12] W. S. Klug, R. F. Bruinsma, J.-P. Michel, C. M. Knobler, I. L. Ivanovska, C. F. Schmidt, and G. J. L. Wuite, Phys. Rev. Lett. **97**, 228101 (2006).
[13] U. S. Schwarz, S. Komura, and S. A. Safran, Europhys. Lett. **50**, 762 (2000).
[14] J. Lidmar, L. Mirny, and D. R. Nelson, Phys. Rev. E **68**, 051910 (2003).
[15] S. Komura, K. Tamura, and T. Kato, Eur. Phys. J. E **18**, 343 (2005).
[16] L. Pauchard, Y. Pomeau, and S. Rica, C. R. Acad. Sci., Ser. IIb: Mec., Phys., Chim., Astron. **342**, 411 (1997).
[17] L. Pauchard and Y. Couder, Europhys. Lett. **66**, 667 (2004).
[18] C. Quilliet, Phys. Rev. E **74**, 046608 (2006).
[19] N. Delorme and A. Fery, Phys. Rev. E **74**, 030901(R) (2006).
[20] C. I. Zoldesi and A. Imhof, Adv. Mater. (Weinheim, Ger.) **17**, 924 (2005).
[21] C. I. Zoldesi, C. van Walree, and A. Imhof, Langmuir **22**, 4343 (2006).
[22] C. Quilliet, C. I. Zoldesi, C. Riera, A. van Blaaderen, and A. Imhof, Eur. Phys. J. E **27**, 13 (2008).
[23] C. I. Zoldesi, P. Steegstra, and A. Imhof, J. Colloid Interface Sci. **308**, 121 (2007).
[24] P. de Pablo, J. Colchero, J. Gomez-Herrero, and A. Baro, Appl. Phys. Lett. **73**, 3300 (1998).
[25] J. E. Sader, J. W. M. Chon, and P. Mulvaney, Rev. Sci. Instrum. **70**, 3967 (1999).
[26] L. Landau and E. Lifshitz, *Course of Theoretical Physics, Vol. 7, Theory of Elasticity* (Butterworth-Heinemann, Oxford, 1997).
[27] A. V. Pogorelov, *Bendings of Surfaces and Stability of Shells* (American Mathematical Society, Providence, 1988), Vol. 72.
[28] R. D. Gregory, T. I. Milac, and F. Y. M. Wan, SIAM J. Appl. Math. **59**, 1080 (1999).
[29] A. Fery, F. Dubreuil, and H. Möhwald, New J. Phys. **6**, 18 (2004).
[30] E. Reissner, J. Math. Phys. (Cambridge, Mass.) **25**, 80 (1946); **25**, 279 (1946).
[31] W. T. Koiter, in *Progress in Applied Mechanics: The Prager Anniversary Volume* (MacMillan, New York, 1963), pp. 155–169.
[32] C. I. Zoldesi, Ph.D. thesis, Utrecht University, 2006.
[33] M. F. Ashby, *Materials Selection in Mechanical Design*, 2nd ed. (Elsevier, Amsterdam, 1999).
[34] N. Tsapis, E. R. Dufresne, S. S. Sinha, C. S. Riera, J. W. Hutchinson, L. Mahadevan, and D. A. Weitz, Phys. Rev. Lett. **94**, 018302 (2005).
[35] B. Neumann, B. Vincent, R. Krustev, and H.-J. Muller, Langmuir **20**, 4336 (2004).